Title:	*Second Generation Photogrammetry Project*
Author:	J.A. Crawford
Abstract:	This is the first installment for my second generation photogrammetry project. This approach provides many benefits compared to the original approach as described herein. Version 2.0 includes some grammar changes, but more significantly appends §4 with revised and greatly improved method for mounting the angular encoder, plus §7.
Date:	20 July 2024
Version:	2.0

1 A Change in Direction

After spending a lot of time and effort on my *photogrammetry* project ([1] through [9]), I've decided to switch gears a bit and move toward a telescope more suitable for both astronomy and photogrammetry purposes. This decision is based on several reasons:



Figure 1 Original photogrammetry project, using closed-loop direct-drive azimuth and elevation servo control



Figure 2 Imaging the moon

1. the scope will need to be first calibrated against the night-time star field before it can be used for precision photogrammetry, so astronomical use will actually precede any other use.
2. the original photogrammetry telescope has a number of short-comings including:
    a. the mount is too heavy
    b. the fork mount, owing primarily to the elevation axis arrangement, is not at rigid as I would like
    c. I have concerns about the cogging torque present in the azimuth motor interfering with precise astronomical tracking
    d. the bill of materials cost is larger than I want, in large part due to:

i. expensive optical encoders which are now obsolete, somewhat difficult to obtain, and certainly difficult to align
ii. the 3-phase motor controllers alone are also expensive at about $90 each, and also difficult to obtain
iii. the harmonic drive used for the elevation axes has become overly expensive
1. high-quality harmonic drive components have gone through the roof cost-wise ($500+) since I initiated my photogrammetry project ($120)
2. as attractive as these drives are, I do not want to replicate this cost
iv. the 3-phase motors are fairly expensive (compared to NEMA17s)

3. I want to reduce the cost of materials and general complexity
a. new rotary encoders requiring much less space and at much lower cost are now available, with SPI or I2C interfaces
b. I want to use stepper motors like the NEMA17's for their lower cost, size, and weight if possible.

An important question to address is, "How good is good enough?" A clear answer is vital if the issues just listed are to be satisfactorily addressed. For example, a telescope used for planetary observation / astrophotography must use extremely high magnification as compared to large astronomical objects like the Andromeda galaxy (M31) or my photogrammetry pursuits. Rather, I need to limit the breadth of my efforts and attend to the specific identified objectives. The magnification needed for my original photogrammetry pursuits will be fairly low.

1.1 Performance Objectives

My plan is to build as many as 5 copies of the telescope-plus-mount I'm envisioning. Consequently, cost needs to be constrained. As such, if I go with a refracting telescope I will be limited to about a 3" aperture. On the other hand, if I opt to go with a reflecting-type telescope, my aperture limit is probably more like 6" to 8". My preference for this project effort is to use a refractor for a number of reasons, but this decision does not have to be made now. The diffraction-limited resolution for a 3" aperture is about 2 arc-seconds, which is on par with the best seeing conditions likely to be had.

Relatively wide-field astrophotography begs the use of a small f-number for the telescope, ideally less than 7. Light gathering power is also important for astronomy use. Photogrammetry will primarily be done during daylight hours, so light gathering power is not an issue for that use-case. It will be more important to match the telescope's focal length to the CCD/CMOS sensor's pixel size.

Planetary astrophotography will require a fairly large telescope aperture (e.g., 12 inches), and a relatively long focal length associated with the required high magnification. All of the mechanical features are required to be rock solid because diffraction-limited performance will dictate resolution on the order of 0.5 arc-second (atmospherics will limit this to more like 2 arc-seconds, but image processing could net diffraction-limited performance). This use-case is outside the target objectives for this project.

1.2 High-Level Project Plan

1. Design the mount to use both stepper motors (e.g., NEMA-17) and small 3-phase motors for both axes.
a. 3-phase motors
i. Higher RPMs possible meaning higher telescope angular slew-rates possible
ii. Arbitrarily small angular steps possible
iii. Motors are more expensive.
iv. Motor control will require full 3-phase PWM capabilities like those available in the TMS320F28379D processor from Texas Instruments.
b. NEMA-17 stepper motors
i. Limited to fairly low RPM and consequently low telescope angular slew-rates

   ii. Angular step size typically about 1.8°. Micro-stepping can reduce the step size appreciably, but not without a substantial loss in available motor torque.
   iii. Simple drivers like the A4998 can be used thereby saving cost and reducing design complexity. The NEMA 17 steppers still require a minimum of 12VDC, and preferably at least 18VDC.
   iv. Smaller stepper motors may have sufficient torque, but are generally more expensive than the commonly-used NEMA 17 stepper motor.
2. Make the mount configurable as an Azimuth/Elevation mount, or as an equatorial mount.
3. Use appropriate processors
   a. Stepper motors can be sufficiently served by the Arduino family (e.g., Due) plus A4998 drivers.
   b. 3-phase motors will require the TMS320F28379D or similar plus associated 3-phase motor drivers
4. Design for a maximum telescope weight of 15 pounds plus a 5 pound counterweight.
5. Axes drives are to be friction-drive plus worm gear in nature, for virtually zero backlash, high resolution, and low cost.
   a. A full-size worm gear arrangement (200+ teeth, 4+ inch diameter) is expensive, north of $200 for each axis thereby making this traditional approach unattractive.
   b. A small worm gear set exhibiting a 50:1 reduction ratio can be had for more like $15 on Amazon. Potential backlash and precision issues with the worm gear are reduced by the step-down ratio used within the friction drive portion of the mount.
   c. Shoot for a torque capability of 35 inch-pounds for both axes.
6. Make the mount as rigid as possible.
7. Keep the weight of the mount (less any counter-weights) to less than TBD pounds.

1.3 Game-Changing Technology

Single-chip processors like those used in the Raspberry Pi 5 (Broadcom BCM2712, quad-core, 64-bit 2.4 GHz Arm processor) and ZWO's ASIAIR Pro (Broadcom BCM2711B0, quad-core, 64-bit 1.5 GHz Arm processor) are bringing unprecedented computing power to even small astronomical platforms. All-sky plate-solving[1] capabilities are making expensive angular encoders (like those from Renishaw) all but unnecessary for star field navigation and initial pointing. Precision image-based star tracking is capable of sub-arc-second RMS tracking errors using similar mathematical techniques, thereby enabling arbitrarily long photographic exposures to be made.

Even so, the photogrammetry aspects of my project will still require absolute angular accuracy in order to do precise triangulation on overhead aircraft. Residual errors in the telescope mount will be calibrated out, however, using the astronomical based techniques mentioned earlier.

2 General Concept

A substantial amount of work has already been performed on the new design as evidenced by the work-in-progress shown in Figure 3 and Figure 4. Only the *right ascension* (RA) axis has been completed thus far, but an almost carbon copy of it will also be fabricated for the *declination* (DEC) axis. For terrestrial *azimuth / elevation* use, the right ascension axis will be tilted more horizontally and become the elevation axis where as the declination axis will be used for azimuth axis as shown in Figure 5. In principle the axes-roles could be reversed as shown in Figure 6, but the axis tilt-adjustment would be undesirably stiff and therefore not advocated. The orientation in Figure 5 also results in better motor placement and access to some of the thumb-screws.

[1] Plate-solving entails comparing a built-in star atlas with an arbitrary picture of the star field as seen by the telescope to determine the precise viewing coordinates to within typically less than 0.5 arc-seconds.

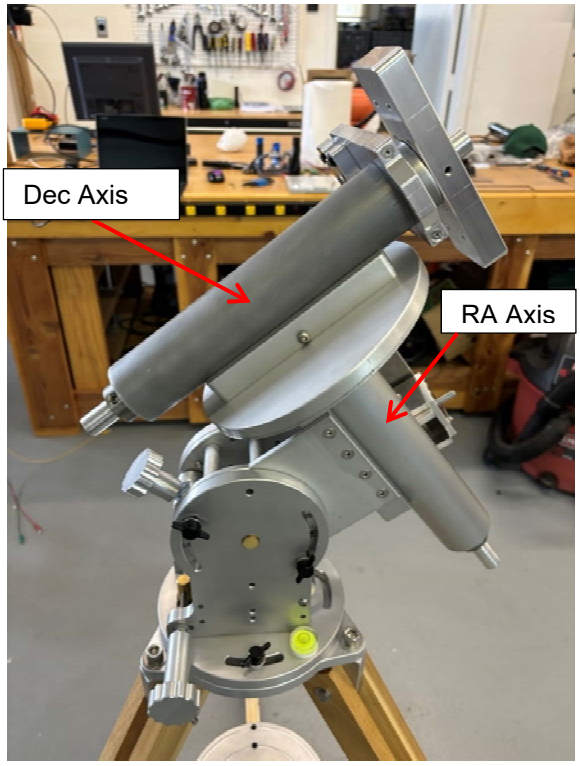


Figure 3 One side of the telescope mount thus far



Figure 4 Opposite side of the telescope showing the 3-phase motor (BLDC-42) for the right-ascension axis

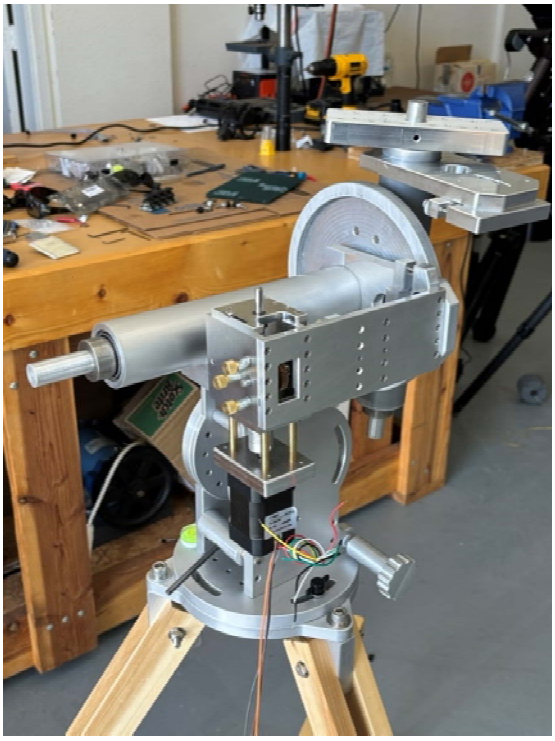


Figure 5 Mount adjusted for azimuth / elevation usage (preferred arrangement)

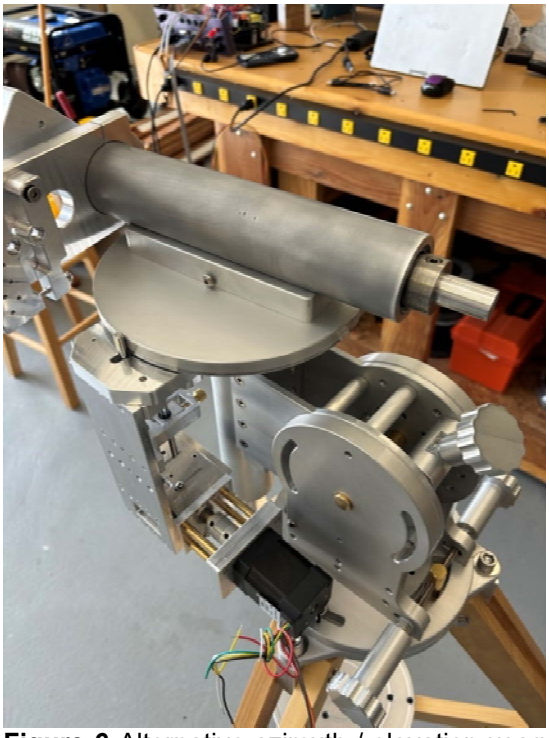


Figure 6 Alternative azimuth / elevation usage, not preferred due to tilt-adjustment stiffness

The double-knobbed control shown in Figure 4 is ideally used once to align the RA axis with the celestial pole in azimuth. Similarly, the single knob control is used to align the RA axis with the celestial pole in elevation.

This mount design utilizes a *friction drive* approach for both the RA and DEC axes. This choice was made because (i) friction drives can exhibit zero backlash and (ii) I wanted to incorporate some novelty into my design. A 6 mm hardened chrome steel axis drives the much larger 7.5" diameter disk as shown in Figure 7 thereby resulting in a *gear-ratio* of about 31.75 : 1.0. The friction drive portion is driven by a 50:1 worm gear arrangement and subsequent motor resulting in a total rotational step-down ratio of 31.75 * 50 = 1,587.503. This large ratio relaxes any backlash issues associated with the worm gear arrangement, and also substantially reduces torque requirements for the drive motors. One down-side to having such a large ratio is, however, that appreciable motor RPM is required if the telescope's pointing angle is to be changed very quickly. More details about the friction drive are provided in the next section.



Figure 7 Close-up of the RA axis friction drive in which a 6 mm hardened chrome steel axle is used to drive the much larger 7.5"diameter disk affording an effective gear-ratio of about 31.75 : 1

3 Friction Drive Details

I purposely avoided high-precision bearings in the drive design in order to keep cost down, but this also led to several mechanical difficulties attributed to sub-thousandth of an inch imperfections. I spent quite a bit of time combatting very small gaps between the drive axle and large disk as shown in Figure 8.

One of the features I incorporated into the design appears to be entirely new. Rather than simply press the drive axle up against the outer perimeter of the main disk which would result in an equal amount of lateral force against the main axis of the large disk, I opted to use a *difference-based* drive approach in which a second chrome steel axle is pressed up against an inner rim-edge of the large disk on the back-side of the disk, having a diameter of 6.5". This approach is purposely intended to keep large lateral forces off of the main axis. Some of the details are shown in Figure 9. (Also see §7.)

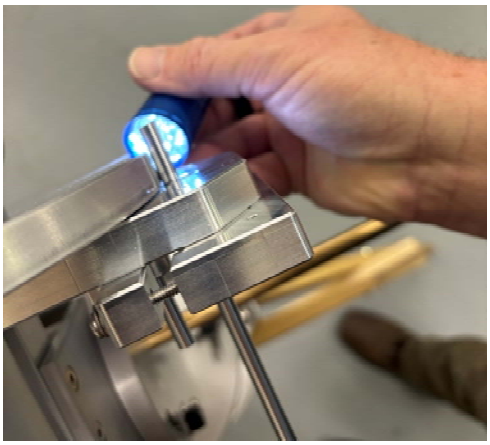


Figure 8 Lateral forces at the drive axle / main disk interface initially led to inadequately small engagement between the two hard surfaces. Note the gap between the axle and main disk over most of the disk's thickness.

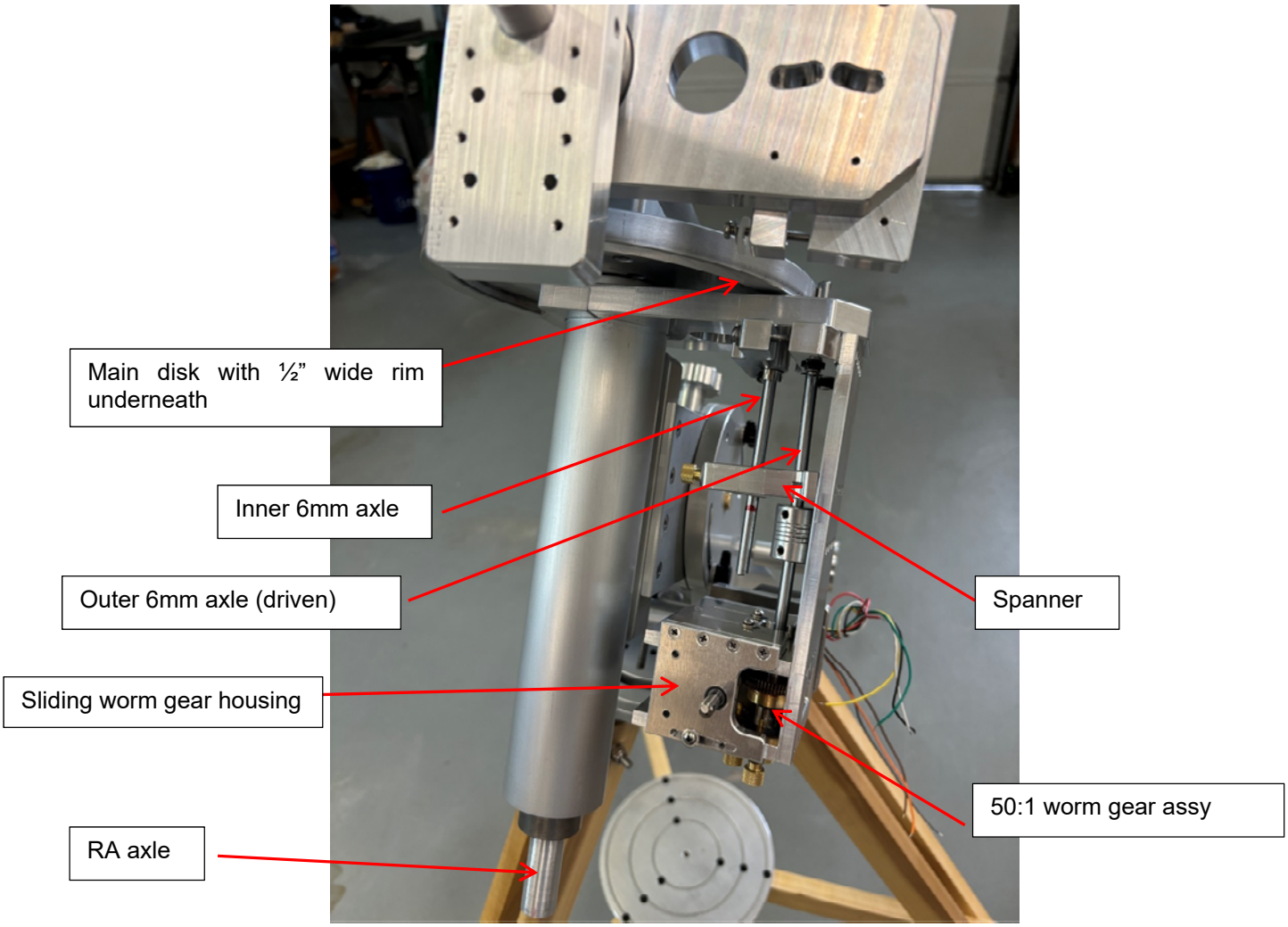


Figure 9 Close-up view of the differential-drive approach used in the friction drive design. The inner 6 mm axle provides outward pressure to the main disk rim whereas the outer (driven) provides and equal put opposite lateral force. The overall *gear ratio* is about 1,588 : 1.

Modeling the interaction between the driven chrome steel axle and anodized 6061 aluminum main disk is not easy. First of all, the lateral forces result in very minute displacement of the ball bearing's axis which gets amplified with distance from the bearing itself. This is the primary mechanism causing the gap shown in Figure 8. Using larger and more expensive bearings would of course help, but modeling information is generally insufficient to predict performance before building the mechanism.

The surface interaction between the chrome steel axle and aluminum disk is itself quite involved. Most friction drives use soft steel for the main disk (which would have seriously impacted weight) or at a minimum 7075 aluminum (which would have impacted cost). I reasoned that elastic deformation of the large 6061 disk's rim would be fine, and would actually increase the contact surface area between the chrome axle and disk.

If the chrome steel axle and main disk were completely non-elastic, the contact *area* between the two would be a perfect infinitesimally thin line. In actuality, a small contact area is created through elastic deformation (primarily of the main disk in this case), thereby limiting the stresses considerably. These contact stresses are called *Hertz contact stresses*, and were first studied by Hertz in 1881 [10].

In the case of contact between two cylinders (the chrome steel axle and the large aluminum main disk), the situation is as shown in Figure 10. The half-width *b* of the rectangular contact area between the two cylinders is given by

$$b = \sqrt{\frac{4F\left(\frac{1-\nu_1^2}{E_1}+\frac{1-\nu_2^2}{E_2}\right)}{\pi L\left(\frac{1}{R_1}+\frac{1}{R_2}\right)}} \tag{1}$$

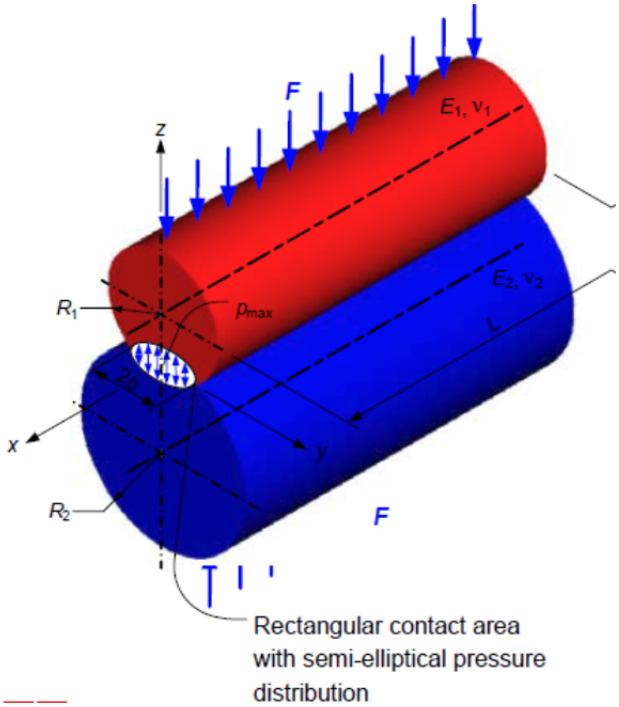


Figure 10 Contact between two cylinders [10]

where E_1 and E_2 are the moduli of elasticity for the two cylinders, and ν_1 and ν_2 are the Poisson's ratios respectively. The length of contact is given by *L*. If cyclinder #1 is assumed to be the chrome steel drive axle, R_1 = 0.50*0.2362" and since it is assumed to be much harder than the 6061 aluminum disk, its

modulus of elasticity will be taken to be ∞ (making v_1 immaterial). For the aluminum disk, R_2 = 3.75" and L will be taken to be 0.50". Using these values in (1) produces

$$b = \sqrt{\frac{4F\left(\frac{1-v_2^2}{E_2}\right)}{13.72}}\ in. \tag{2}$$

The Poisson ratio for 6061 aluminum is about 0.33 whereas its modulus of elasticity is about 68.9 GPa which equates to 10^7 pounds per square inch. This information simplifies (2) further to

$$b = 0.0001612\sqrt{F}\ in \tag{3}$$

Taking F = 50 pounds as a rough guess at this point, the half-width of the contact region is only about 0.00114" which is not discernable to the unaided eye. A fairly simple derivation of (1) can be found in *Wikipedia* under the term *contact mechanics*.

The result given by (3) provides strong evidence that the rotational axis of the main disk and chrome steel axle must be aligned as nearly parallel as possible. Any angular error will result in the contact area being less than optimal and the total friction between the two surfaces being less than desired. This value for b at a distance of 1" (about the distance from the bearing to the top of the contact region) represents an angular error of only 0.065^o !

After a fair amount of investigation and some trial and error , I reasoned that the best way to stay with the inexpensive ball bearings I had chosen and still deal with the realities of (3) was to pre-stress the two chrome steel 6mm axles as sketched out in Figure 12 and shown in Figure 11. The Spanner shown in Figure 11 was used to impress lateral pressure on the two chrome steel axles, using the (hidden) ball bearings[2] as fulcrums thereby purposely bending the axles ever so slightly in order to get good contact between the axles and the main disk's rim (both inside and out). The Spanner was used to force the two axles slightly apart on the lower side of the fulcrum points which then pushed the axles together on the top side of the fulcrum points thereby pinching the large disk's rim in between. This arrangement *floats* the two-axle assembly in order to avoid imposing lateral forces on the main telescope axis.

The line-forces involved can be fairly high, and care must be exercised not to employ more lateral force on the ball bearings than they can handle. Over tightening the Spanner's action on the axles can actually break the ball bearing(s).

The slight axle bending introduced by the Spanner caused a slight mis-alignment between the drive axle and the rest of the housing; notably the worm drive assembly. This was compensated for using a flexible coupler as shown in Figure 11. I was a fortunate beneficiary of the 3D printing world as the axles and flexible coupler primarily serve that hardware realm.

[2] Each of the recessed ball bearings is held in place by a high-precision pocket situated on the top-side of each of the swivel arms shown in Figure 11. Since the swivel arms each moved with respect to their own singular axes, these acted to effectively pinch the rim of the large disk between the two axles.

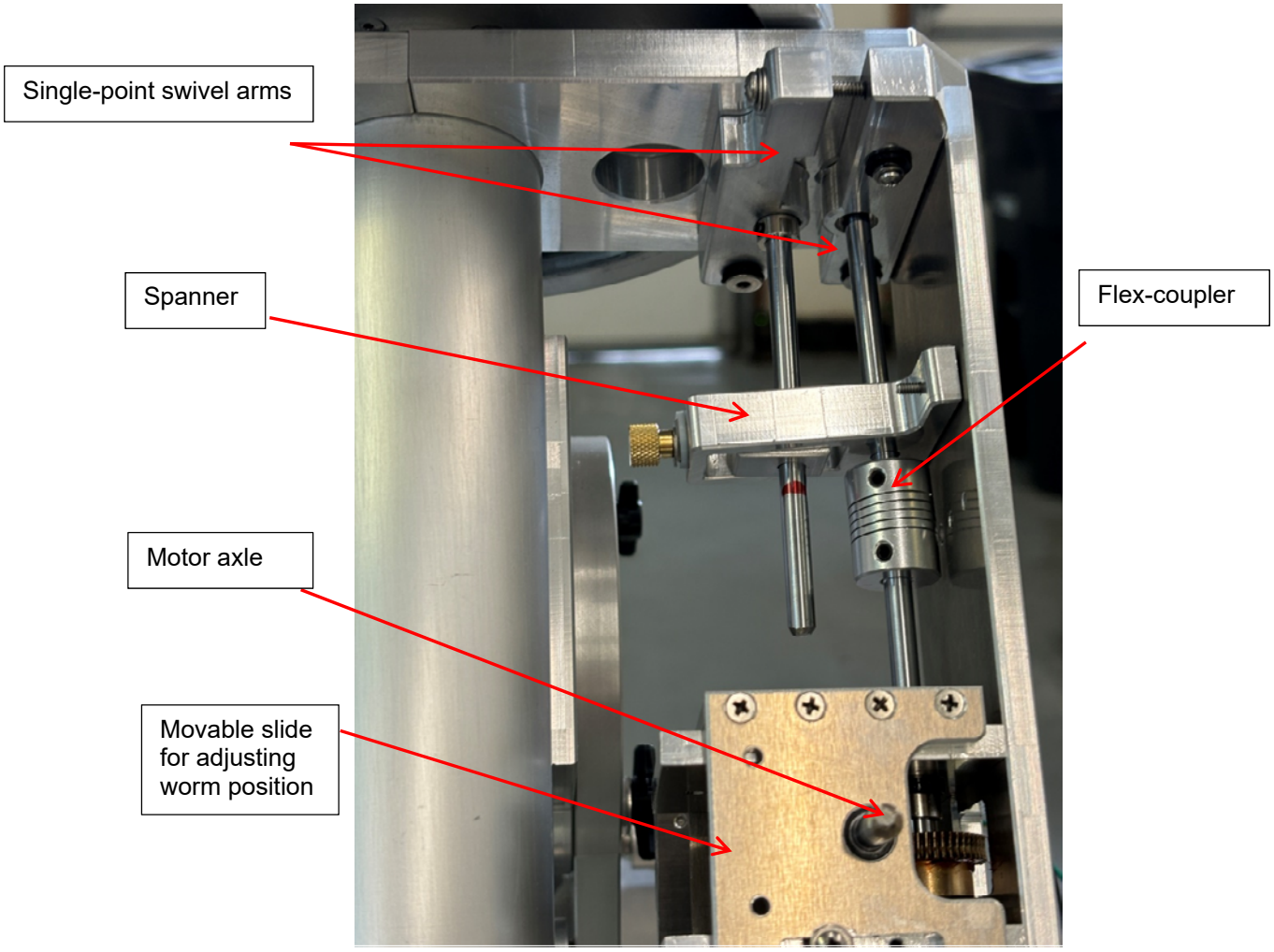


Figure 11 Close-up of the pivot arms holding the axle ball bearings

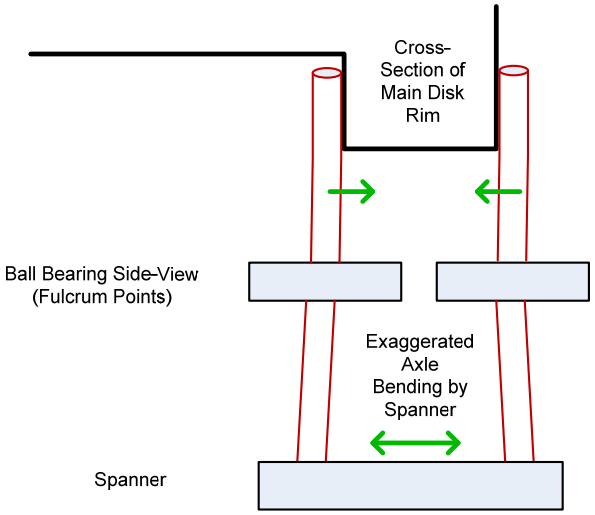


Figure 12 Ball bearings serve dual purposes: (i) means for low-friction axle rotation and (ii) fulcrum points to convert axle-separation from the Spanner into axle-squeezing action about the main disc's rim

3.1 Worm Gear Assembly

The worm gear assembly must mate up with the chrome steel axle as already discussed. In addition, it must permit the worm and worm-gear to be meshed in a fairly precise way in order to (i) minimize wear on the gears, (ii) minimize backlash, and (iii) keep rotational losses low. Two views of the worm/worm-gear assembly are shown in Figure 13 and Figure 14.

The assembly shown in Figure 14 consists of (i) a vertical section which carries the entire floating differential drive arrangement, (ii) two small horizontal shelves bolted to the vertical section, and (iii) a moveable cage arrangement which has the worm integrated within and ultimately supports the drive-motor. Two window regions are purposely included in the aluminum housing in order to make alignment between the worm and worm-gear straight forward to visually accomplish.

An angle-encoder will be supported by the three adjustable bolts shown at the bottom in Figure 13. The encoder must be precisely positioned in all three dimensions in order to work in an optimal manner. More details about the encoder are provided in §4.

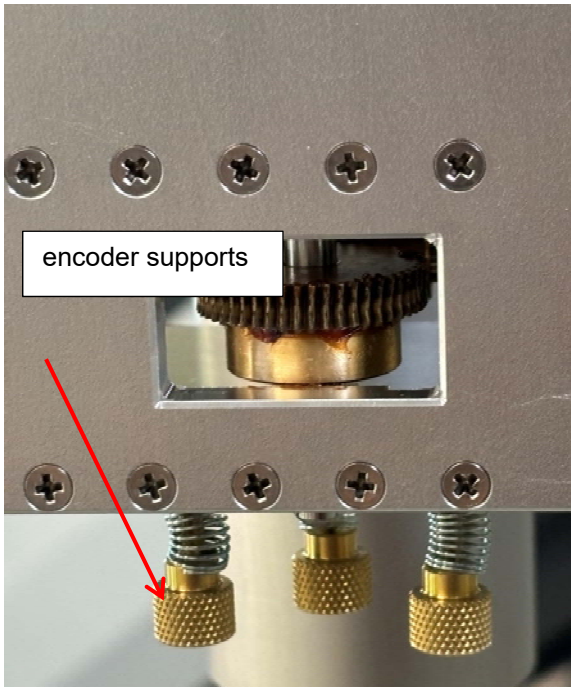


Figure 13 Side view of worm gear, with magnetic encoder mounting bolts shown below

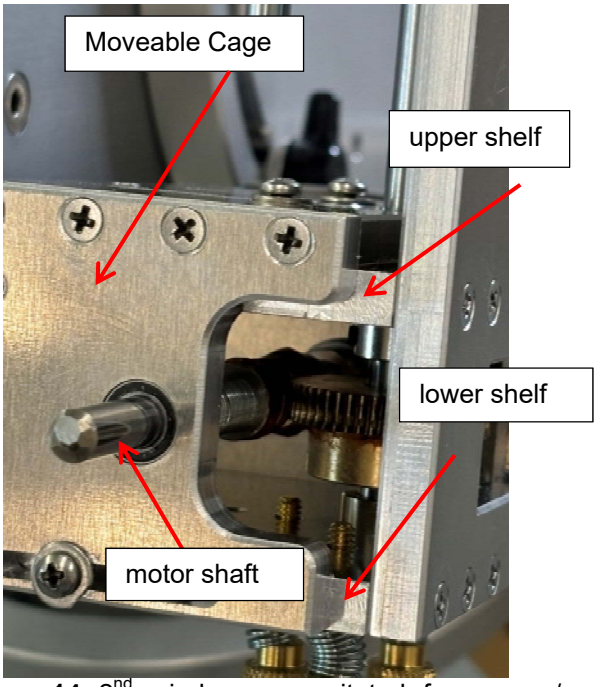


Figure 14 2nd window necessitated for worm / worm-gear mating alignment

4 Angle Encoder

The angular encoder I used in the original design ([1] – [9]) was very difficult to align, fairly expensive, physically large, and entailed communicating over a complicated external interface which had to be serviced by the TI DSP. In addition, the original has become obsolete. The encoder industry seems to have split into two camps, one camp being extremely expensive and high-performing (20+ bits, thousands of dollars each), and the other camp much less expensive with considerably lower performance. Since cost-containment is one of my main objectives, I adopted the latter device family for this effort.

The angle encoder in this design is connected to the drive axle of the friction drive. As such, there is a 31.75:1 step-down in the telescope's angular position versus that which the encoder sees. This is equivalent to almost 5 additional bits of angular resolution over that provided by the encoder itself.

The encoder I have adopted for this project is the AS5048 magnetic encoder which ideally provides 14-bits of angular resolution. Combining this with the step-down ratio of the friction drive produces a net resolution of almost 19 bits. In terms of astronomical telescope positioning, this equates to about 2.47 arc-seconds. This is not sufficient for high-precision astronomical closed-loop motor control, but it is more than sufficient for initial pointing. For my original photogrammetry pursuits, this is equivalent to a measurement raster size of about 0.63 feet at a distance of 10 miles; more than adequate, especially when mathematical smoothing and model-fitting (e.g., Kalman) will be used.

The measurement error performance of the AS5048 is, shall we say, not outstanding. My plan is to use calibration against the night-time star field to ferret out errors in the telescope mount and this encoder.

The air-gap between the AS5048 single-chip encoder and magnet (fixed atop the drive shaft) must ideally be maintained within about ±33.5 thousandths of an inch as shown in Figure 16. Lateral alignment between the magnet and AS5048 should ideally be better than about ±0.1 inches as shown in Figure 17, but could be more relaxed depending upon calibration methods.

Control and read-out for the AS5048 encoder will be done over a SPI interface.

The AS5048 can be operated from a 3.3V or 5V supply. The sampling rate needs to be between 10.2 ksps and 12.4 ksps which corresponds to a serial clock rate of about 10 MHz. The encoder's output noise is about 2.73 LSBs (RMS).

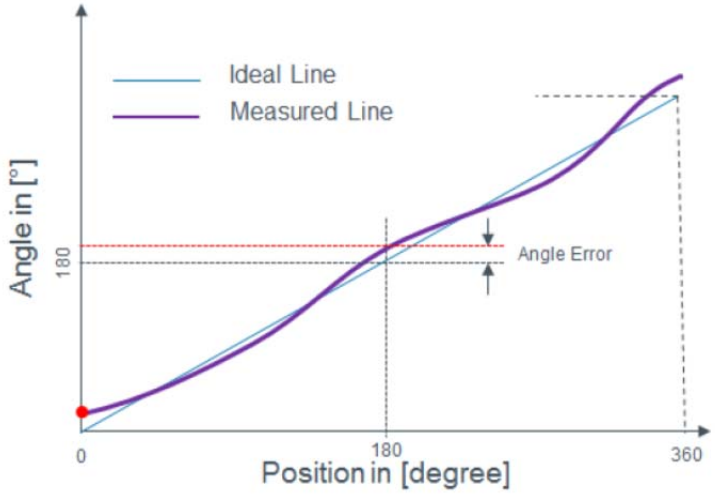


Figure 15 Non-linearity of the AS5048's angular output[3]

[3] Figure 7 of [11].

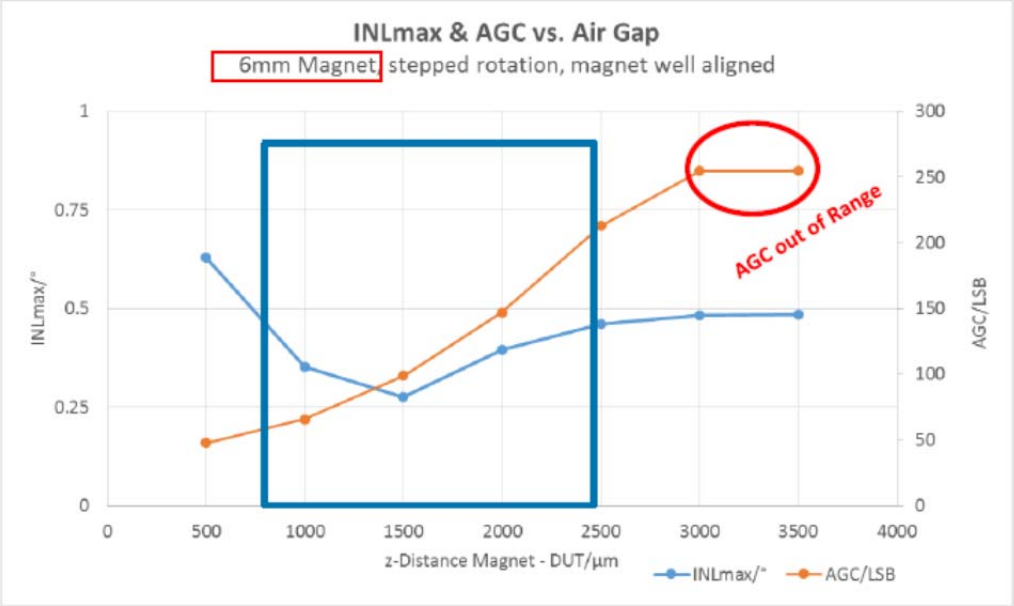


Figure 16 Nonlinearity and automatic gain control as a function of magnet-chip air-gap[4]. The nominal air-gap should be 1650 ± 850 µm (or equivalently 0.065 ± 0.0335 inches).

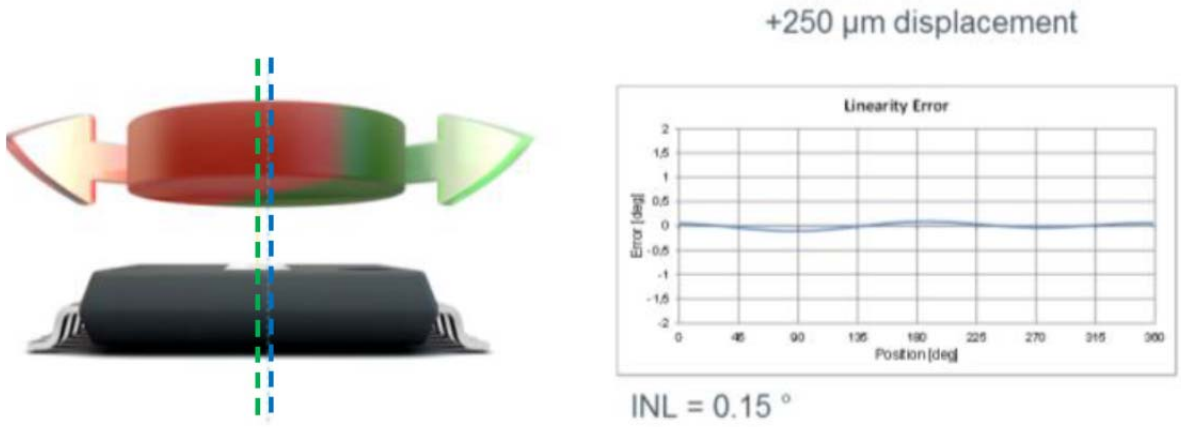


Figure 17 Lateral placement[5] of the magnet with respect to the AS5048 should ideally be within ± 0.098 inches

The spring-loaded 3-point mounting of the angular encoder shown in Figure 13 proved to be mechanically unacceptable because it was not rigid enough nor accurate enough. The approach ultimately adopted makes use of fixed-length rigid posts (which firmly fix the encoder's placement in the (x, y)), and a metal cap which fits over the chrome steel axis for carrying the small magnet. The vertical position of the cap is easily adjusted by hand and the final position secured using a small set-screw as shown in Figure 18 and in the final hardware as shown in Figure 19.

[4] Figure 10 of [11]
[5] Figure 12 of [11]

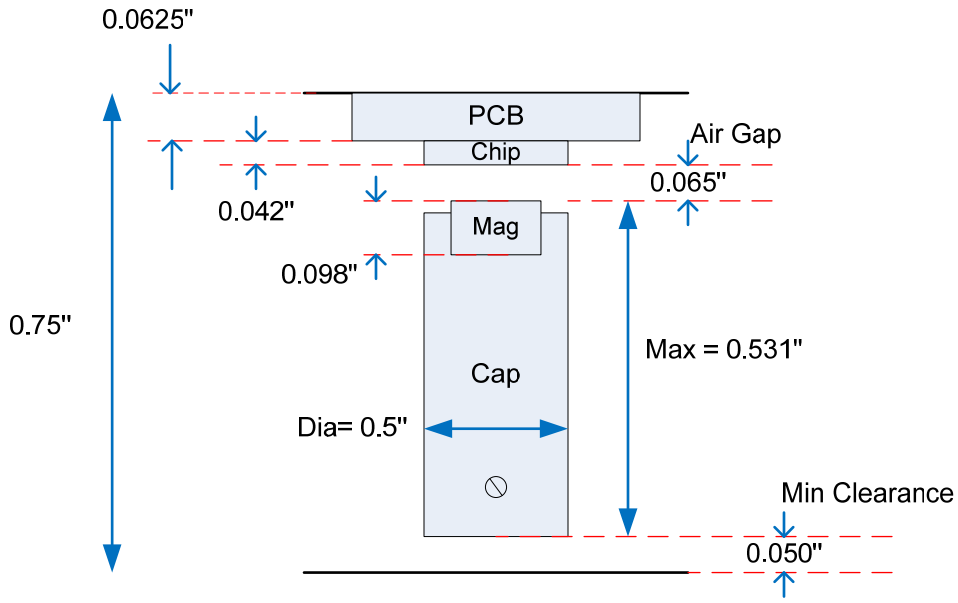


Figure 18 Dimensioning for axle-cap which holds the encoder's disk-magnet[6]

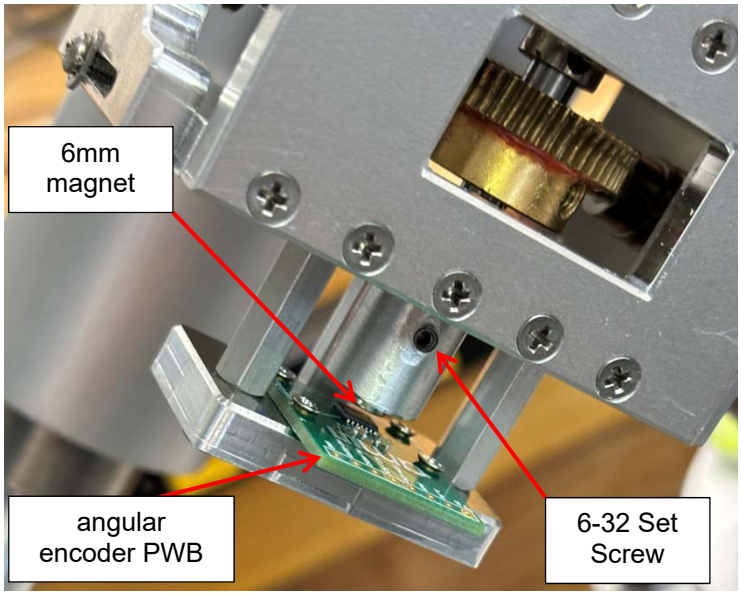


Figure 19 Angular encoder installed at the end of the RA axis

[6] From U29401_Friction_Drive_Configuration.vsd.

5 Next Steps

Immediate next steps include:

- Mount the magnetic encoder for the RA axis and write supporting DSP code to command and query it.
- Using open-loop control of the 3-phase RA axis motor, sinusoidally modulate the RA angle with a laser pointer attached to the mount. Examine the laser-spot at a distance of about 100 yards for smooth operation and repeatability.
- Once a telescope can be attached to the mount, open-loop track a night-time star to more rigorously assess motion smoothness of the RA axis.
- Once these foregoing steps have been successfully achieved, replicate a friction drive assembly for the Dec axis.

6 References

1. J.A. Crawford, “Photogrammetry for Non-Invasive Terrestrial Position/Velocity Measurement of High-Flying Aircraft- Part 7,” August 2023.
2. _____, “Photogrammetry for Non-Invasive Terrestrial Position/Velocity Measurement of High-Flying Aircraft- Part 6AB,” October 2022.
3. _____, “Photogrammetry for Non-Invasive Terrestrial Position/Velocity Measurement of High-Flying Aircraft- Part 6A,” January 2022.
4. _____, “Photogrammetry for Non-Invasive Terrestrial Position/Velocity Measurement of High-Flying Aircraft- Part V: Optical Encoder Completion and Transition to TI DSP,” January 2021, U24933.
5. _____, “Photogrammetry for Non-Invasive Terrestrial Position/Velocity Measurement of High-Flying Aircraft- Part V,” U24933, January 2021.
6. _____, “Photogrammetry for Non-Invasive Terrestrial Position/Velocity Measurement of High-Flying Aircraft- Part IV: Optical Encoder and Elevation Drive,” U24933, August 2020.
7. _____, “Photogrammetry for Non-Invasive Terrestrial Position/Velocity Measurement of High-Flying Aircraft- Part III,” U24933, November 2019.
8. _____, “Photogrammetry for Non-Invasive Terrestrial Position/Velocity Measurement of High-Flying Aircraft- Part II, Direct-Drive Motors,” U24933, April 2019.
9. _____, “Photogrammetry for Non-Invasive Terrestrial Position/Velocity Measurement of High-Flying Aircraft- Part I,” 2017, U24866.
10. Ziaoyin Zhu, “Tutorial on Hertz Contact Stress,” 1 Dec. 2012, OPTI 521, U29017.
11. AMS OSRAM, “AN5000 Rotary Magnetic Position Sensors,” Sept. 28, 2016.

7 Appendix: Friction Drive Support

There are two distinctly different methods possible for conveying rotation from a driven axis to the large friction disk. The first approach applies inward-directed radial forces as shown in Figure 20 and Figure 21. If the forces involved do not vectorially add to zero, a net lateral force will be impressed on the mount-axis which can result in precision issues because the axis-bearing will not be evenly loaded. There are, however, some implementation advantages to having all of the bearings & axles in contact with the *external* perimeter of the friction disk.

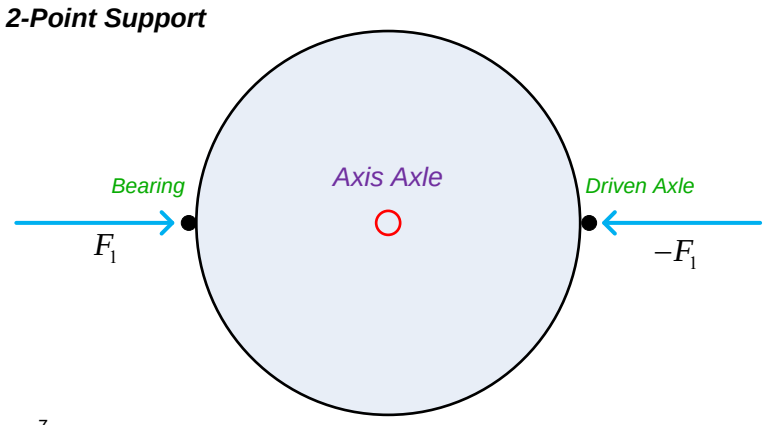


Figure 20 2-point support[7]. Any imbalance in compressive radial forces will result in a net lateral force being imposed on the main axis.

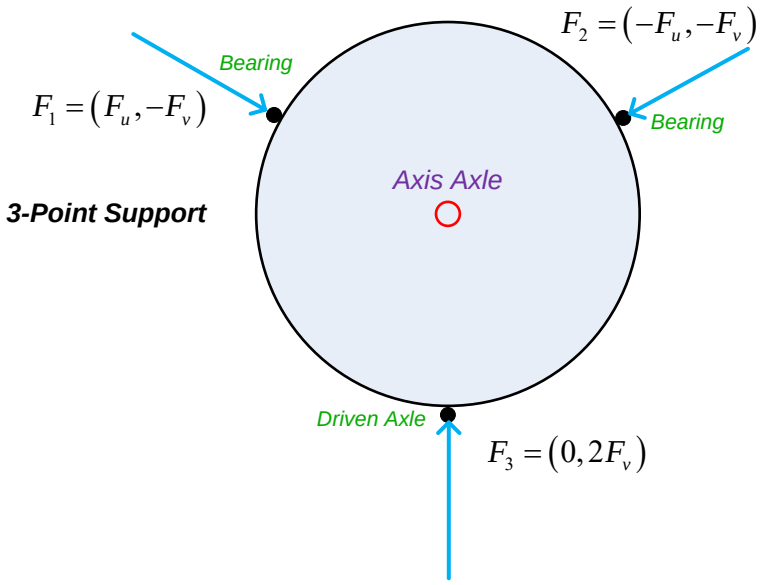


Figure 21 3-point support. Any error in the compressive radial forces will result in a net lateral force being imposed on the main axis in *any* direction.

[7] U29401_Friction_Drive_Configurations.vsd.

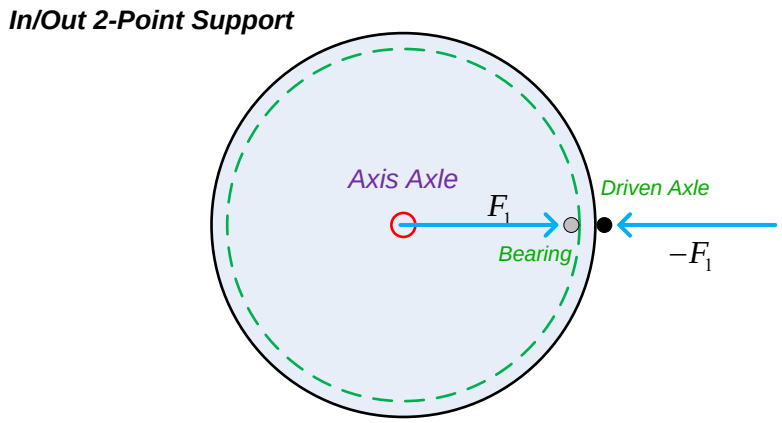


Figure 22 2-point in/out support. In this approach a rim is formed in order to permit complimentary forces to be applied to the rim, thereby all but completely eliminating any net lateral force on the main axle.

7.1 Friction Disk Smoothness Effect on Angle

The bearing and driven-axle supports referred to in Figure 22 are shown in Figure 11 with a simplified sketch of the arrangement further detailed in Figure 23. The driven axle is held by a *pivot arm* which is pseudo-free to rotate about a fixed point and at a fixed distance *d* as shown in Figure 23. Due to minute changes in the fixed disk's radius *R* due to smoothness or other imperfections, the radius may change very slightly, however, as the friction disk is rotated. The following discussion considers how minute changes in *R* affect the friction disk's angular position θ.

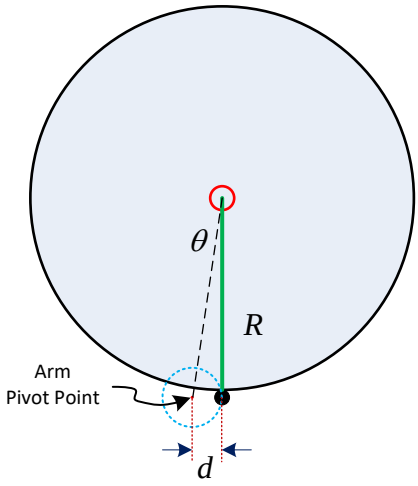


Figure 23 Drive axle is situated a distance *d* away from a fixed pivot point, with the friction disk of radius *R*

Ideally, the pivot arm and radius *R* form an ideal right-triangle. Only the center of the friction disk and the arm pivot point are assumed to be ideally positioned in this discussion. A small change in the disk radius δr introduces a small change in the pivot arm's angle φ as shown in Figure 24 because the length of the pivot arm is a constant. For small changes,

$$\varphi = \frac{\delta r}{d} \tag{4}$$

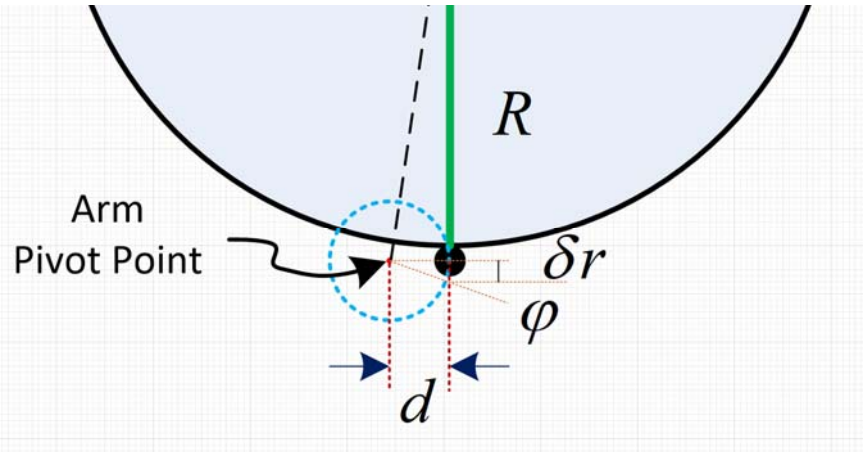


Figure 24 Close-up of Figure 23

Due to the non-zero angle φ, the apparent length of the pivot arm as viewed from the main axis is reduced by

$$\begin{aligned}\delta d &= d\left[1-\cos(\varphi)\right] = 2d\,\frac{1-\cos(\varphi)}{2} \\ &= 2d\sin^2\left(\frac{\varphi}{2}\right) \to 2d\left(\frac{\varphi}{2}\right)^2\end{aligned} \tag{5}$$

Substituting (4) into (5) results in

$$\delta d = 2d\left(\frac{1}{2}\frac{\delta r}{d}\right)^2 = \frac{(\delta r)^2}{2d} \tag{6}$$

Once again assuming small angular changes, the net change in angle θ is finally given by

$$\delta\theta = \frac{\delta d}{R} = \frac{(\delta r)^2}{2dR} \tag{7}$$

Example Calculation:

Assume that the pivot arm length is 2”, the friction disk radius is 3.75”, and the friction disk radius variation is 0.002”. From (7), this roughness would translate into an angular variation of only about ± 0.055 arc-seconds which is completely acceptable.